frontiers | Frontiers in Physics

TYPE Original Research
PUBLISHED 05 August 2025
DOI 10.3389/fphy.2025.1603556

OPEN ACCESS

EDITED BY
Andrea Gonzalez-Montoro,
Polytechnic University of Valencia, Spain

REVIEWED BY
Nicolaus Kratochwil,
University of California, Davis, United States
Eric Harmon,
LightSpin Technologies, United States

*CORRESPONDENCE
K. Herweg,
katrin.herweg@lfb.rwth-aachen.de
S. Gundacker,
stefan.gundacker@cern.ch

RECEIVED 31 March 2025
ACCEPTED 16 June 2025
PUBLISHED 05 August 2025

CITATION
Herweg K, Schulz V and Gundacker S (2025) Analyzing the time distribution of external cross-talk for an SiPM-based TOF-PET detector.
Front. Phys. 13:1603556.
doi: 10.3389/fphy.2025.1603556

Analyzing the time distribution of external cross-talk for an SiPM-based TOF-PET detector

K. Herweg [1,2]*, V. Schulz [1,2,3,4,5] and S. Gundacker [1,6]*

[1]University Hospital RWTH Aachen, Aachen, Germany, [2]Institute of Imaging and Computer Vision, RWTH Aachen University, Aachen, Germany, [3]Hyperion Hybrid Imaging Systems GmbH, Aachen, Germany, [4]Physics Institute III B, RWTH Aachen University, Aachen, Germany, [5]Fraunhofer Institute for Digital Medicine MEVIS, Aachen, Germany, [6]Institute of High Energy Physics, Austrian Academy of Sciences, Vienna, Austria

In the pursuit of developing the fastest time-of-flight positron emission tomography (ToF-PET) detectors, understanding and minimizing noise factors that significantly influence the timing performance of such detectors are vital. Currently, state-of-the-art ToF-PET detectors are silicon photomultiplier (SiPM)-based scintillation detectors, which introduce SiPM-specific noise sources, such as cross-talk. Cross-talk can occur in three scenarios, namely, direct, delayed, and external cross-talk. Although there have been technological developments to address direct and delayed cross-talk, external cross-talk remains challenging to study because it often gets combined with the signal and other noise sources. This work aims to deepen our understanding of external cross-talk by measuring its probability and time distribution across different detector configurations. For this purpose, we conduct dark count measurements with high-frequency electronics and an oscilloscope for readout. We investigate two Broadcom NUV-MT SiPMs, one with 2×2 mm^2 and one with 3.8×3.8 mm^2 active area, and couple each to three bismuth germanium oxide (BGO) crystals of different lengths (3 mm, 15 mm, and 20 mm) wrapped in Teflon. Additionally, we test the SiPM without coupling, with direct Teflon™ wrapping and coupled with the 3 mm crystal without wrapping. Our findings indicate that adding a reflector significantly increases the cross-talk in scintillation detectors. The cross-talk probability increases by a factor of 1.4 to 1.9, with the lower end of this range corresponding to the coupling with the longest crystal (20 mm). Our setup successfully resolved the shift in cross-talk arrival time for crystals 15 mm and longer. Additionally, we have found that the minimal delay time for 15 mm and 20 mm crystals corresponds to the time taken for passing through the crystal twice and that changes in signal slope only occur after this delay time. This behavior is observed for crystals of any size in a few-photon measurement.

KEYWORDS

SiPM, cross-talk, scintillator, TOF, BGO, PET, optical

1 Introduction

In the last two decades, silicon photomultipliers (SiPMs) have become the standard photosensor for positron emission tomography (PET) [1–10] due to their high gain, compactness, and cost-effectiveness. They find significant application in the current search for the fastest time-of-flight PET (TOF-PET) detectors [11] owing to their continuously improved timing capabilities [5], [11–15].

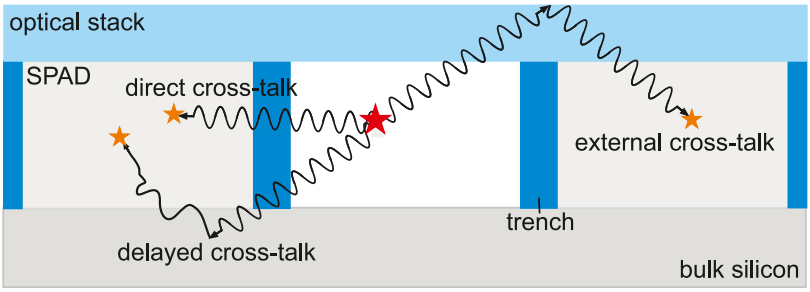

FIGURE 1
Sketch of an SiPM cross-section describing the three different cases of cross-talk. Direct cross-talk directly traverses SPAD borders and trenches (dark blue) and triggers an avalanche in the neighboring SPAD (light gray). Delayed cross-talk is absorbed in the SiPM bulk silicon (dark gray), which triggers a delayed avalanche in the neighboring SPAD. Lastly, external cross-talk leaves the silicon completely and is reflected from the surface of the SiPM coverglass or a crystal coupled to the SiPM (optical stack, light blue) into the neighboring SPAD, where it triggers an avalanche. Inspired by [27] under CC BY 4.0.

SiPMs consist of an array of single-photon avalanche diodes (SPADs) which are connected in parallel and operated in the Geiger mode. There are two possible modes of readout for these SPADs: an analog SiPM, where the sum of signals over all connected SPADs is read out and then digitized in a separate circuit, often an application-specific integrated circuit (ASIC), e.g., NINO [16, 17], TOFPET2 [17–20], or FastIC [17, 21, 22], and a digital SiPM, where each SPAD is digitized individually [5, 6], [23–26]. In both of these readouts, we encounter cross-talk, which contributes significantly to signal deterioration [14, 26, 27].

Cross-talk occurs in all SPAD-based devices and originates from optical photons, which are created by each avalanche through hot intra-band luminescence [28]. There are three different types of cross-talk based on the photon's interactions before being detected in the sensor (see Figure 1). First, if the cross-talk photon travels through the silicon and triggers an avalanche in a different SPAD of the same SiPM, it is called internal or direct cross-talk [14, 27, 29]. Second, if the cross-talk photon is absorbed in the bulk of a different SPAD and therefore causes a delayed avalanche, it is called a delayed cross-talk [14, 27]. Third, if the cross-talk photon leaves the silicon sensor and is detected after being reflected from the cover glass or crystal coupled to the silicon, it is considered to be external cross-talk [2, 27, 29].

Two of these types of cross-talk have been recently addressed by FBK and Broadcom using metal trenches in between SPADs (NUV-MT SiPMs), which absorb internal and delayed cross-talk photons [30]. Thus, external cross-talk remains as a significant contributor to noise, whose reduction and performance influence has recently been investigated by [31, 32]. Since external cross-talk travels through the optical stack (cover glass, coupling, and scintillator) of a scintillation detector, it is delayed compared to the original avalanche. Depending on the optical stack, this delay of the external cross-talk could impact the timing performance of scintillation detectors.

The impact of delayed cross-talk is especially detrimental in applications where few photons are detected, e.g. Cherenkov radiation. Cherenkov radiation is an alternative to scintillation to further improve the timing performance in TOF-PET. Recently, many investigations have been made into using the Cherenkov radiation of bismuth germanium oxide (BGO) for improving timing performance [9, 15], [33–38]. In BGO detectors, the combination of scintillation and Cherenkov radiation in addition to the few Cherenkov photons makes it challenging to achieve ultra-fast timing performance. The DIGILOG project [38, 39] aims to use finely segmented SiPMs or μSiPMs and a semi-digital electronics approach to detect the timing of the first arriving photons, i.e., Cherenkov photons. Measurement of the first photons is achieved by choosing a sufficiently high segmentation of the SiPM to measure few photon or single-photon signals, which are likely to be affected by external cross-talk.

In this work, we extend the knowledge available on external cross-talk probability and time distribution based on different optical stacks. We also discuss whether external cross-talk can be distinguished from true events and corrected for. For this purpose, we conduct dark count measurements and time-resolved cross-talk measurements with power-efficient high-frequency (HF) electronics [9, 40, 41] as a readout for NUV-MT SiPMs of different sizes coupled to BGO crystals of different lengths.

2 Materials and methods

In this work, we measured the cross-talk of two differently sized Broadcom NUV-MT SiPMs, AFBR-S4N22P014M and AFBR-S4N44P014M (both with 40 µm micro cell pitch and typical breakdown voltage of 32.5 V 2×2 mm^2 [42] and 3.8×3.8 mm^2 [43]

TABLE 1 Crystal and SiPM configurations used in measurements.

2×2 mm^2	3.8×3.8 mm^2	Wrapping
No crystal	No crystal	No wrapping
No crystal	No crystal	Teflon™ cover
$2 \times 2 \times 3$ mm^3 BGO	$3 \times 3 \times 3$ mm^3 BGO	No wrapping
$2 \times 2 \times 3$ mm^3 BGO	$3 \times 3 \times 3$ mm^3 BGO	Teflon™
$2 \times 2 \times 15$ mm^3 BGO	$3 \times 3 \times 15$ mm^3 BGO	Teflon™
$2 \times 2 \times 20$ mm^3 BGO	$3 \times 3 \times 20$ mm^3 BGO	Teflon™

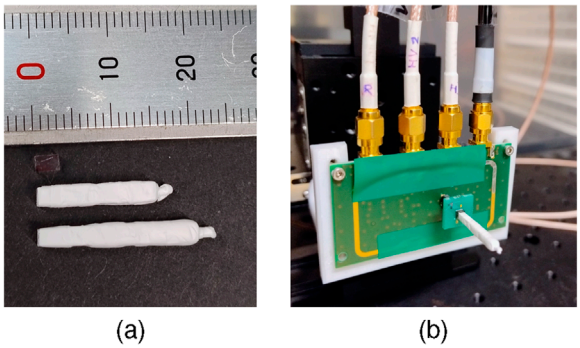

FIGURE 2
(a) shows the three different crystal lengths with a cross-section of 2 × 2 mm^2, while **(b)** presents an exemplary measurement setup with a 20 mm long BGO crystal glued to the 2 × 2 mm^2 SiPM. The SiPM is plugged into the HF readout board, which in turn is connected to the oscilloscope and power supplies.

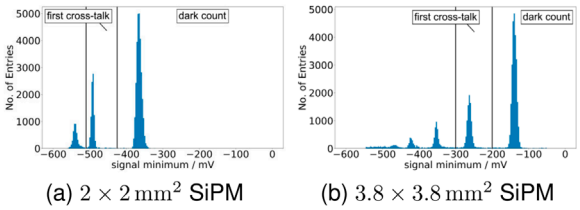

FIGURE 3
The histogram of the signal minimum for the 2 × 2 mm^2 SiPM with no crystal or wrapping at 45 V bias voltage in **(a)** and for the 3.8 × 3.8 mm^2 SiPM with the same optical stack and bias voltage in **(b)**.

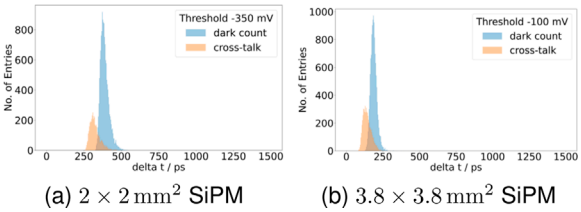

FIGURE 4
The histograms of time differences between the first timing threshold of −30 mV and the secondary threshold of−350 mV **(a)** or −100 mV **(b)** for dark count (blue) and cross-talk events (orange). The 2 × 2 mm^2 SiPM with no crystal or wrapping at a secondary threshold of −350 mV is shown in **(a)** The 3.8 × 3.8 mm^2 SiPM with no crystal or wrapping at a secondary threshold of −100 mV is visible in **(b).** Both measurements were conducted at 45 V bias voltage.

active area), with different configurations of crystals and wrapping (see Table 1). BGO crystals (Epic Crystal, China) of 3 mm, 15 mm, and 20 mm length were coupled with Meltmount (n = 1.582, Cargille, USA) and measured either without wrapping or with Teflon™ wrapping (see Figure 2).

Measurements were conducted with the timing channel of an HF readout, as described in [9, 40, 41] (see Figure 2b), and an oscilloscope (LeCroy Waverunner 9404M-MS, bandwidth 4 GHz, 20 GS/s) for digitization. The setup was put in a temperature-controlled dark chamber at 16°C. All measurements were conducted for four different bias voltages (40 V, 43 V, 45 V, and 47 V).

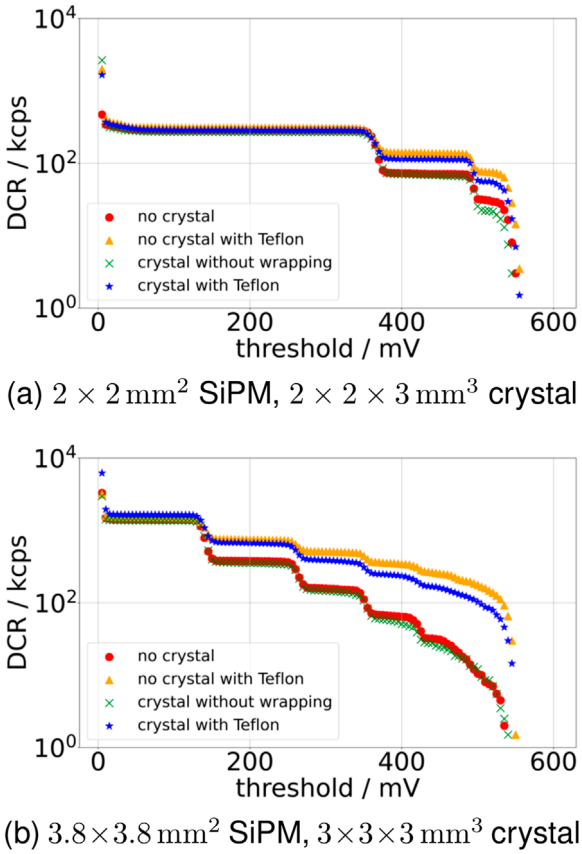

FIGURE 5
Development of the DCR and cross-talk probability over different thresholds at 45 V bias voltage for different optical stacks for **(a)** the SiPM and **(b)** the SiPM. Wrapping the 3 mm crystal or the SiPM itself in Teflon™ increases the cross-talk significantly, while just adding a naked 3 mm long crystal to the optical stack contributes to no significant difference in terms of the detected cross-talk.

2.1 Dark count scans

To determine the dark count and cross-talk behavior for different SiPM and crystal configurations, we set a low threshold on the falling edge of the timing signal, which has a negative polarity. We then collected waveforms in the time range of 2 ms for each bias voltage investigated. In post-processing, a variable threshold was applied to the waveforms, and the number of threshold crossings on the falling edge of the signals was counted. The number of threshold crossings is a measure of the overall dark count rate (DCR). In order to estimate the cross-talk probability, the ratio between the first and second photo electron levels of the DCR was calculated [13, 29, 44].

2.2 Time-resolved cross-talk measurement

For estimating the time distribution of cross-talk photons, we measured the time difference (Δt_{thres}) between a fixed threshold of −15 mV or −30 mV on the falling edge of the signal and a second threshold lower on the falling edge, which was varied between −50 mV and −500 mV. In addition to this time difference, we also extracted the signal minimum (see exemplarily for 45 V Figure 3), which was

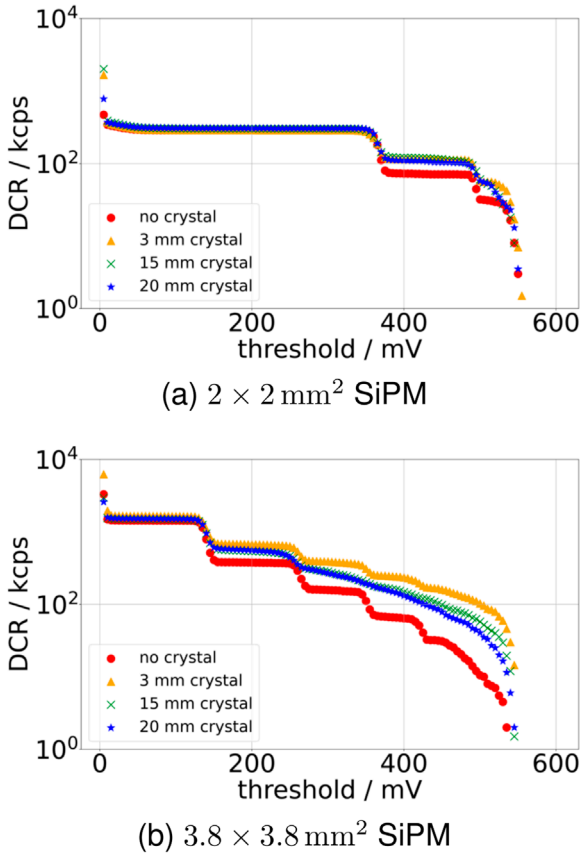

FIGURE 6
The development of the DCR over different thresholds at 45 V for different crystal lengths coupled to the SiPM. **(a)** shows the behavior of the 2 × 2 mm^2 SiPM, while **(b)** displays the 3.8 × 3.8 mm^2 SiPM. The cross-talk is increased for all crystals coupled but experiences a slight reduction with an increase in crystal length.

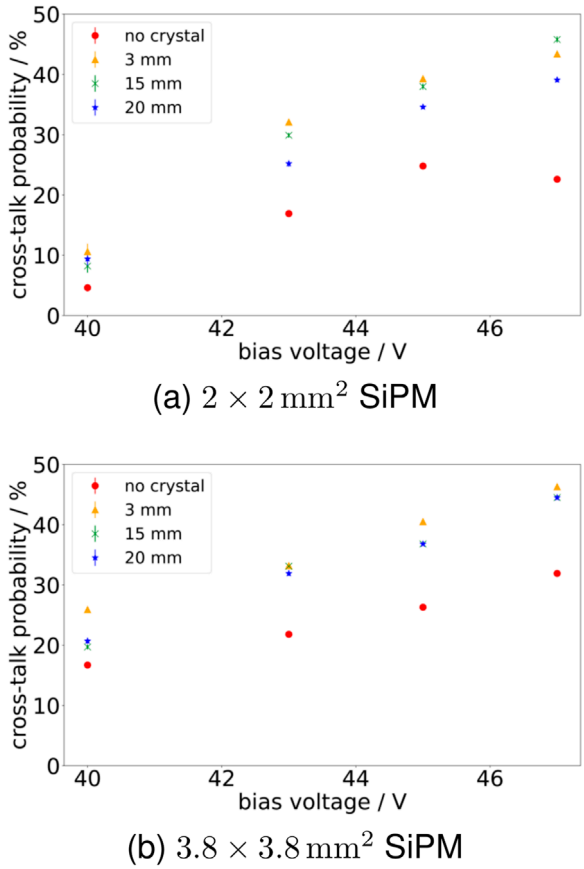

FIGURE 7
Cross-talk probability for different bias voltages. **(a)** Shows the 2 × 2 mm^2 SiPM, where bias voltages are found to increase monotonously, except for the highest bias voltage with no crystal coupling, where saturation seems to occur. For the 3.8 × 3.8 mm^2 SiPM **(b)**, monotonous increase was observed for all bias voltages.

used as an energy filter to distinguish between dark counts and cross-talk events. Figure 3a shows the 2 × 2 mm^2 SiPM displaying a highly non-linear behavior, which will be addressed in the *Discussion*.

After filtering to dark count and cross-talk events (see Figure 3), the respective time difference distributions (see Figure 4) were fitted with a Gaussian curve, and the mean and the full width at half maximum (FWHM) were extracted.

3 Results

3.1 Dark count rates and cross-talk probability

Investigating the changes in the measured DCR based on different optical stacks, it can be seen that, although adding a crystal without wrapping does not significantly change the DCR at different thresholds, adding a reflector like Teflon™ to the optical stack either directly on top of the SiPM or wrapped around the coupled crystal significantly increases the cross-talk (see Figure 5 for 45 V bias voltage). This observation holds for SiPM sizes and all bias voltages. The cross-talk probability for the 45 V bias voltage is increased from 24.8 ± 0.4% (2 × 2 mm^2 SiPM) or 26.3 ± 0.3% (3.8 × 3.8 mm^2 SiPM) for the SiPM without wrapping to 39.3 ± 0.5% or 40.5 ± 0.7% for the SiPM with a 3-mm crystal and wrapping. If the SiPM is directly wrapped with Teflon™, the increase in cross-talk probability is even slightly higher compared to the crystal wrapped in Teflon™ with 44.8 ± 0.8% and 49.3 ± 0.7%, respectively.

While comparing Teflon-wrapped crystals of different sizes in terms of the DCR, it is notable that the cross-talk probability decreases more strongly for the longer crystals than for the shorter ones (see Figure 6). This effect is especially visible in Figure 6b for the 3.8 × 3.8 mm^2 SiPM, but is observed for both SiPMs.

For the different bias voltages investigated, we could observe an overall increase in cross-talk probability for the 3.8 × 3.8 mm^2 SiPM (see Figure 7b). The 2 × 2 mm^2 SiPM, on the other hand, displays a decreased cross-talk probability for the measurement without the crystal and the highest bias voltage (see Figure 7a). We believe this outlier is caused by limitations of our readout electronics approach.

3.2 Time-resolved cross-talk measurement

For the 2 × 2 mm^2 SiPM without crystal or wrapping, the measured time differences for dark counts and first cross-talk at

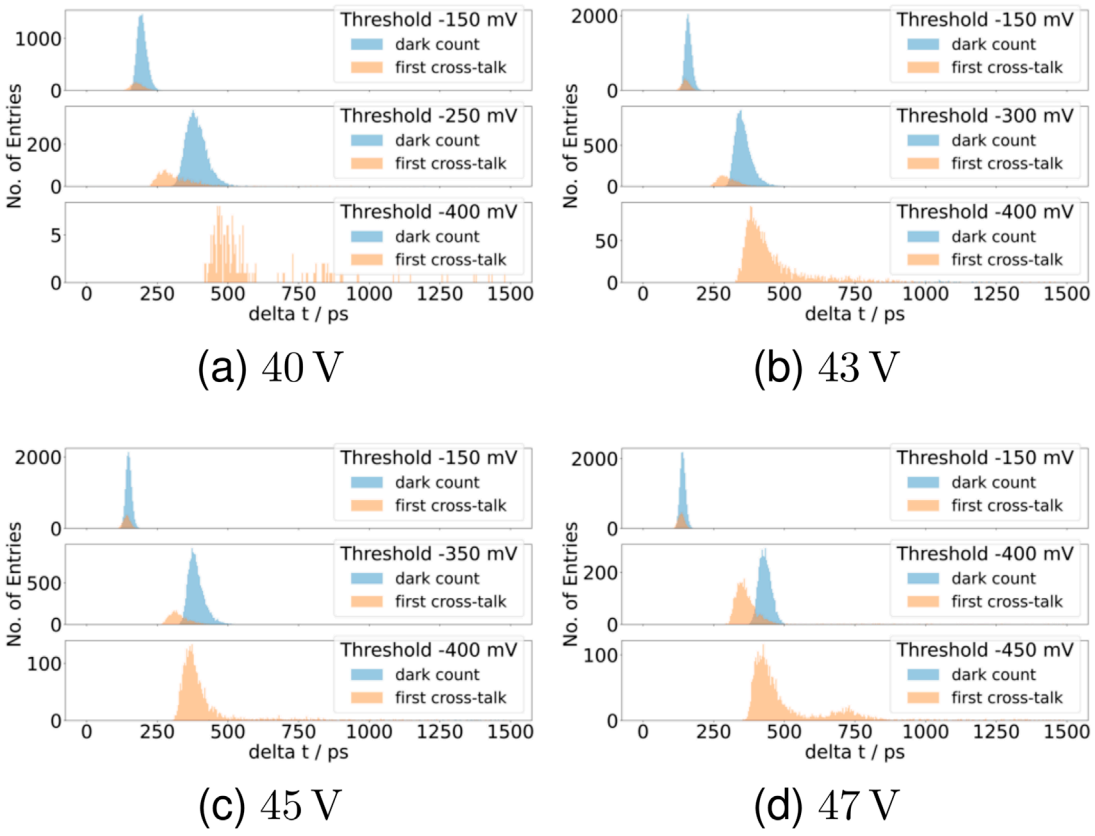

FIGURE 8
Time differences between different thresholds on the falling edge of the signal for the 2×2 mm^2 SiPM without crystal or wrapping. Different bias voltages are shown.

three different thresholds can be seen in Figure 8 for all bias voltages. It is notable that at a threshold of −150 mV, the time difference distribution for the first cross-talk overlaps completely with the distribution of dark counts for all bias voltages. With an increase in the threshold, we observe a separation between the cross-talk and dark count distributions, from −250 mV for 40 V bias voltage to −400 mV for 47 V bias voltage. When thresholds exceed the single SPAD amplitude, only cross-talk photons remain, which reduces statistics, and also the width of the time difference distributions significantly increases. For further investigations, a bias voltage of 45 V was chosen to have sufficient statistics in the cross-talk. The higher bias voltage of 47 V does not provide significantly higher statistics, which was already shown in Figure 7a. In addition, the time difference distribution at a threshold of −450 mV for 47 V shows a small second peak at roughly 750 ps, which can be related to a waveform artifact caused by limitations in our readout electronics approach. So although the peak separation at −400 mV is more distinct (see Figure 8d) for 47 V compared to 45 V, we continued measurements with 45 V.

Considering now a bias voltage of 45 V and coupling crystals of different lengths to the 2×2 mm^2 SiPM (see Figure 9), it can be seen that the shape and position of time difference distributions for the first cross-talk photons change with introduction of a crystal and an increase in its length. While we observed a slight shift of the cross-talk photon distribution towards the dark count distribution for the 3 mm crystal, this shift is much increased for the 15 mm and 20 mm crystal (see Figure 9a), so that the cross-talk distribution completely overlaps with the dark count distributions for these crystal lengths. For thresholds higher than the single SPAD amplitude, we see only cross-talk photons contributing to a time difference distribution. In addition, the width of the time difference distribution significantly increases and has changed shape for the 15 mm and 20 mm crystals.

For the 3.8×3.8 mm^2 SiPM, the trend of broadened and shifted time difference distributions for longer crystals and higher thresholds is similar to that of the 2×2 mm^2 SiPM (see Figure 10). The main difference is the lower single SPAD amplitude so that all thresholds need to be reduced compared to the 2×2 mm^2 SiPM to show the same effects. In addition, thresholds over −250 mV suffer from low statistics and wide distributions.

We plot the mean of the time difference distributions for dark counts and first cross-talk photons separately (see Figure 11). The error on the means in Figure 11 was chosen to represent the FWHM of the distributions in order to detect the threshold at which cross-talk and dark counts can be distinguished from each other based on the calculated time difference or fall time. For both SiPMs, the mean of the dark count and cross-talk distributions diverge from a common starting point for the measurement with no crystal and

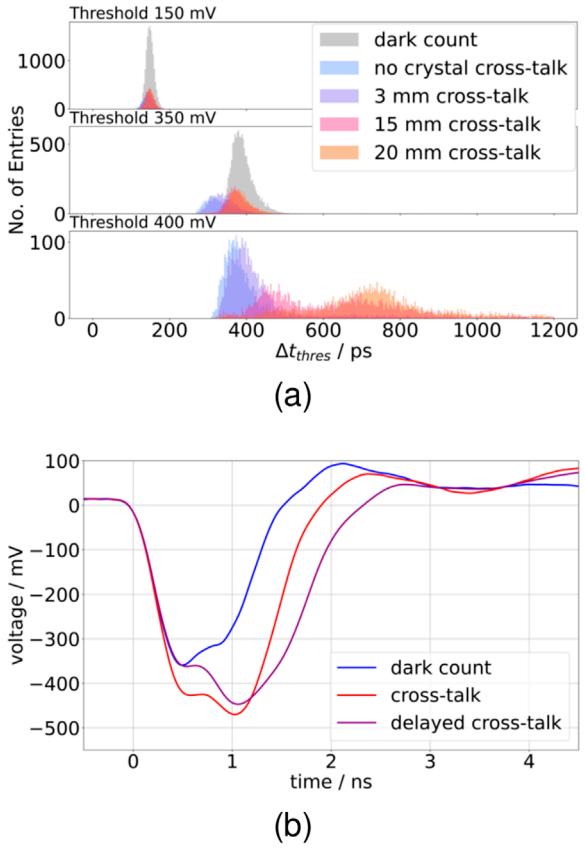

FIGURE 9
Time differences between different thresholds on the falling edge of the signal for the 2×2 mm^2 SiPM at 45 V bias voltage. Different crystal lengths are shown in **(a)** Some exemplary waveforms calculated as the average over 500 measurements can be seen in **(b)** The difference between a direct and delayed cross-talk is clearly visible.

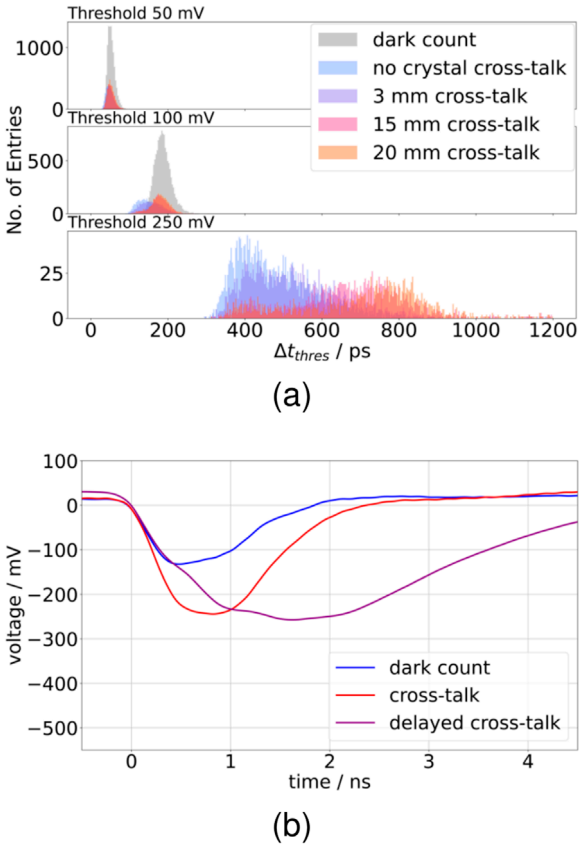

FIGURE 10
Time differences between different thresholds on the falling edge of the signal for the 3.8×3.8 mm^2 SiPM at 45 V bias voltage. Different crystal lengths are shown. Different crystal lengths are shown in **(a)** Some exemplary waveforms calculated as the average over 500 measurements can be seen in **(b)** The difference between a direct and delayed cross-talk is clearly visible.

Teflon™ wrapping (see Figures 11a,b). For the 2×2 mm^2 SiPM, dark counts and cross-talk show distinct distributions from a threshold of −325 mV, while for the 3.8×3.8 mm^2 SiPM, this threshold lies at −100 mV. When a 20 mm crystal is added to the optical stack, it can be seen (Figures 11a,b) that the cross-talk photon's distribution behaves similarly to the dark count distribution. We would expect most of detected cross-talk photons to pass through the length of the crystal at least twice before being detected again, which for the 20 mm BGO crystal corresponds to a time delay of roughly 280 ps. The measurements show that with HF readout, the 3.8×3.8 mm^2 SiPM can only reach this time difference for a threshold higher than the single SPAD amplitude. For the 2×2 mm^2 SiPM, a time difference of 280 ps is reached at a threshold of approximately −275 mV. The 2×2 mm^2 SiPM might show a slight deviation in the cross-talk behavior from the behavior of dark counts above −275 mV. Considering the 2×2 mm^2 SiPM with the 3 mm and 15 mm crystals, we see no significant change between the SiPM directly wrapped in Teflon™ and coupled with the 3 mm crystal (see Figure 11a), which also has a low expected delay time of 42 ps. For the 15 mm crystal on the other hand (see Figure 11a), a significant difference in the time difference distributions of dark counts and cross-talk is visible above the delay time of 210 ps.

4 Discussion

4.1 Dark count rates and cross-talk probability

The measured DCR and cross-talk probability fall in the same order of magnitude, as stated in the Broadcom datasheets [42, 43]. A slight deviation in the DCR from the datasheet can be explained through the lower temperature in our setup during measurements (16°C in our case compared to 25°C in the datasheet). Measuring the DCR for different optical stacks, we have found that the reflector increases the detected cross-talk more in comparison to adding of a crystal or changing the crystal length (see Figure 5), which fits well to results presented by Gola et al. [45] and Kratochwil et al. [46]. Once a reflector is added to the optical stack, the probability to detect cross-talk increases at the maximum by a factor of 1.9. However, once a crystal is introduced, the cross-talk probability decreases

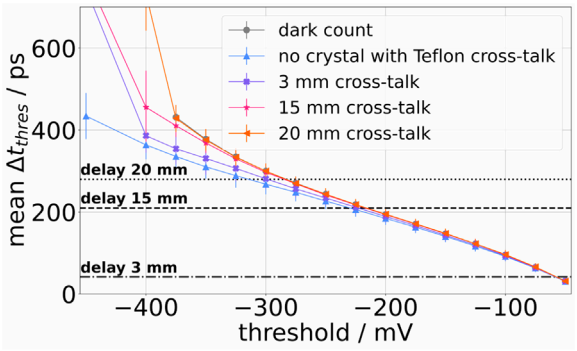

(a) $2 \times 2\,\mathrm{mm}^2$

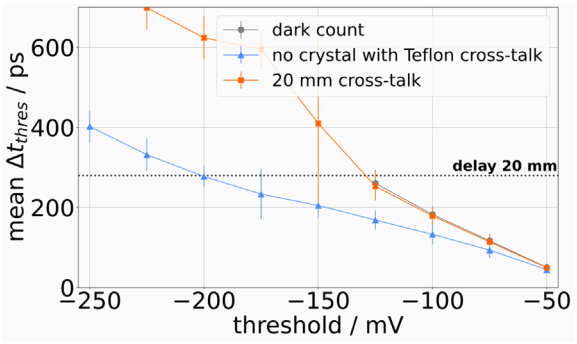

(b) $3.8 \times 3.8\,\mathrm{mm}^2$

FIGURE 11
Mean time differences plotted against different thresholds on the falling edge of the signal for the 2×2 mm^2 SiPM in **(a)** and the 3.8×3.8 mm^2 SiPM in **(b)** We compare the SiPM directly wrapped in Teflon™ with the 3 mm crystal wrapped in Teflon™, the 15 mm and the 20 mm crystal. All measurements were conducted at 45 V bias voltage.

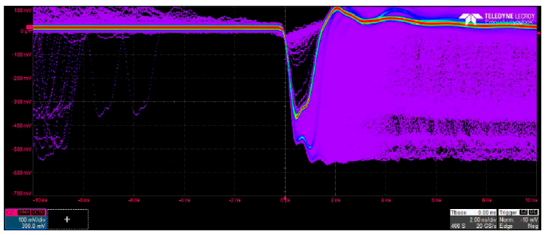

(a) $2 \times 2\,\mathrm{mm}^2$, no crystal

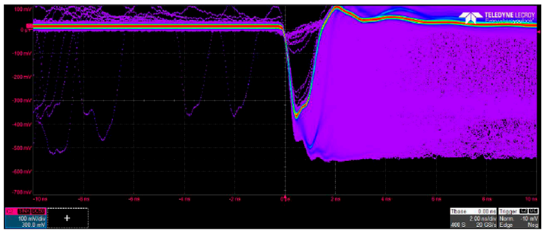

(b) $2 \times 2\,\mathrm{mm}^2$, 20 mm

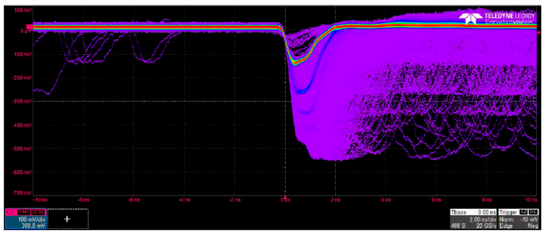

(c) $3.8 \times 3.8\,\mathrm{mm}^2$, no crystal

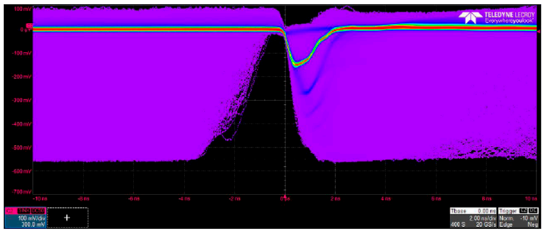

(d) $3.8 \times 3.8\,\mathrm{mm}^2$, 15 mm

FIGURE 12
Waveforms for no crystal and 20 mm crystal on the 2×2 mm^2 SiPM at 45 V bias voltage in **(a,b)** respectively, while **(c,d)** show waveforms for the 3.8×3.8 mm^2 SiPM with no crystal and the 15 mm crystal. For both SiPMs, the shift in the cross-talk is visible. The double-peak structure visible in **(a,b)** does not appear in **(c,d)**.

with an increase in crystal length (see Figure 6b). The similarity of cross-talk probability between no crystal and crystal without wrapping is due to the Broadcom NUV-MT SiPMs being covered by a protective window, which presents a first change in the medium for the cross-talk photons. Since Meltmount and crystal have a low refractive index mismatch with the cover glass, this transition has less influence on the cross-talk probability compared to the reflector choice and crystal length. For crystals of 20 mm length, often used in clinical scanners, the cross-talk is only increased by a factor of 1.4. The decrease in the cross-talk probability aligns with physical principles, as the lateral sides of the crystal offer pathways for cross-talk photons to escape the detector. The same effect is also evident in the reduced statistics observed at higher thresholds in the time-resolved cross-talk measurements.

As observed in Figure 6b, for the measurements with crystals, the DCR steps are more smeared out compared to the SiPM without crystal. In addition, it is apparent that this smearing is more prominent for the longer crystals. We believe that this behavior is caused by a variation in the arrival time of the cross-talk photons, which, depending on when in relation to the primary dark count the cross-talk is detected, will change the signal amplitude for a multi-photon signal.

4.2 Time-resolved cross-talk measurement

In the time-resolved cross-talk measurements, we have discovered that with our measurement setup, we can identify a difference in fall time between a measurement with and without a crystal, if the crystal is sufficiently long and the expected delay of cross-talk photons therefore long enough. We could see this difference for both 15 mm and 20 mm BGO crystals (see Figure 9) using both SiPMs. The shift can also be observed in Figure 12, where the delay of the cross-talk photons when measuring with a 20 mm (see Figure 12b) or a 15 mm (see Figure 12d) crystal is visible in the waveforms.

The time difference distributions of cross-talk photons for the most part show as a single peak distribution. In the singular case where a second peak occurs (see Figure 8d), a higher time difference is observed than for the main peak. This double-peak structure appears to be an artifact of the readout electronics, likely attributable to saturation and bandwidth limitations. This hypothesis is supported by the absence of the double peak in the 3.8×3.8 mm^2 SiPM, which exhibits a significantly smaller signal amplitude. We deduce from the single-peak structure of cross-talk photons that a majority of cross-talk photons passes into the crystal, where they experience delay. The different interfaces in the optical stack seem to have a higher probability of refraction over reflection. For the cover glass–crystal interface, this effect is observed due to the photons passing from an optically less dense into an optically denser material, which means no total reflection is expected, and the ratio between reflection and refraction is dependent on the incidence angle, which is limited by the detector geometry. Considering the interface between SiPM and cover glass, we do not know the exact optical configuration. Therefore, we cannot make definitive assumptions on reflection and refraction. However, the results of our measurements suggest that this interface also favors refraction over reflection for cross-talk photons.

When the SiPM is directly wrapped in Teflon™, the difference in the cross-talk and dark count time difference distributions for even small thresholds (see Figures 11a,b) shows that the cross-talk photons arrive almost instantly. Therefore, events with cross-talk have a significantly steeper rising edge, which is also visible in Figures 9b, 10b, 12. When a 15 mm or 20 mm crystal is coupled (see Figures 11a,b), we can see that until the time difference mean surpasses the minimal delay of crystal photons, the falling edge stays the same for both cross-talk and dark count events. We thus believe that the majority of cross-talk photons indeed travel into the crystal and thereby accumulate a delay of at least 280 ps for 20 mm crystals or 210 ps for 15 mm crystals. Although we cannot see a strong deviation between dark counts and cross-talk for both SiPMs with the 20 mm crystal, we can see a deviation for the 2×2 mm^2 SiPM with the 15 mm and the 3 mm crystal. For the 3 mm crystal, the delay time is comparatively small at 42 ps, which means that the difference to the SiPM with direct Teflon™ wrapping is negligible. However, the delay time for the 15 mm crystal at 210 ps ensures that the cross-talk photons do not impact the fall time before the delay but cause a significant deviation in fall time for the cross-talk events after the minimum delay time. We consider this proof that indeed cross-talk photons will at the minimum travel twice the crystal length before being detected by the SiPM.

Regarding fast timing for ToF-PET, this means that in a few-photon measurement with fast signal rise time, as expected for the DIGILOG project [38, 39], cross-talk should not impact the first-photon timing performance significantly as long as thresholds below the expected arrival time of cross-talk photons are chosen. For readouts with slower rise time or bandwidth limitations, cross-talk might still impact the rising edge of the signal even before their expected arrival time. Additionally, if we want to acquire more information than the first-photon timestamp, direct and delayed external cross-talk could combine with later arriving photons, making it difficult to determine the time structure of an event. Further studies are necessary to investigate these possibilities.

5 Conclusion and outlook

In this work, we have quantified that only adding additional optically transparent materials, though with a different refractive index, does not significantly increase the probability to detect cross-talk. For a significant increase, a reflector must be added to the optical stack of the detector. Using a reflector, at most a 1.9-fold increase in the measured cross-talk can be expected for a Broadcom NUV-MT SiPM, independent of its size. In addition, the increase in measured cross-talk decreases with increasing crystal length, down to a 1.4-fold increase of the measured cross-talk for a 20 mm crystal.

The time-resolved measurements have shown that, with the HF readout, it is possible to resolve the shift in cross-talk arrival time when coupling crystals of 15 mm or 20 mm length. Additionally, we found that most of the cross-talk signals travel at the minimum twice the length of the coupled crystal before being detected by the SiPM. For both 15 mm and 20 mm crystals, we showed no significant influence of the delayed cross-talk on timing if the threshold is below the expected minimum delay of the cross-talk photons. We expect a similar behavior for crystals of any size. This relation has so far only been shown in a few-photon measurement. If it holds for multi-photon measurements as well, is still to be determined.

As a continuation of this work, a more elaborate measurement setup with a laser as the start signal could be considered to provide a more highly resolved measurement. It is important to note the limitations of our current readout electronics approach, which present challenges that are not easily overcome. Further investigation is needed, possibly with reduced gain performance, to achieve a clearer understanding of the timing aspects of external cross-talk and to mitigate saturation effects.

Data availability statement

The raw data supporting the conclusions of this article will be made available by the authors, without undue reservation.

Author contributions

KH: conceptualization, data curation, formal analysis, investigation, methodology, software, writing – original draft, and writing – review and editing. VS: writing – review and editing. SG: conceptualization, investigation, supervision, and writing – review and editing.

Funding

The author(s) declare that financial support was received for the research and/or publication of this article. This research is funded by the Deutsche Forschungsgemeinschaft (DFG, German Research

Foundation) - 500540345 and the Swiss National Foundation (SNF) - #200021L_208073. Open access funding was provided by the Open Access Publishing Fund of RWTH Aachen University.

Acknowledgments

The authors declare the following financial interests/personal relationships which may be considered potential competing interests with the work reported in this paper: VS is the co-founder and employee of the spin-off company Hyperion Hybrid Imaging Systems GmbH, Aachen, Germany.

Conflict of interest

Author VS is co-founder of and employed by Hyperion Hybrid Imaging Systems GmbH.

The remaining authors declare that the research was conducted in the absence of any commercial or financial relationships that could be construed as a potential conflict of interest.

Generative AI statement

The author(s) declare that no Generative AI was used in the creation of this manuscript.

Publisher's note

All claims expressed in this article are solely those of the authors and do not necessarily represent those of their affiliated organizations, or those of the publisher, the editors and the reviewers. Any product that may be evaluated in this article, or claim that may be made by its manufacturer, is not guaranteed or endorsed by the publisher.

References

1. Kim CL, Wang GC, Dolinsky S. Multi-pixel photon counters for tof pet detector and its challenges. *IEEE Trans Nucl Sci* (2009) 56:2580–5. doi:10.1109/TNS.2009.2028075

2. Spanoudaki VC, Levin CS. Photo-detectors for time of flight positron emission tomography (tof-pet). *Sensors (Switzerland)* (2010) 10:10 484–505. doi:10.3390/s101110484

3. Nassalski A, Moszynski M, Syntfeld-Kazuch A, Szczesniak T, Swiderski L, Wolski D, et al. Multi pixel photon counters (mppc) as an alternative to apd in pet applications. *IEEE Trans Nucl Sci* (2010) 57:1008–14. doi:10.1109/TNS.2010.2044586

4. Yamaya T, Mitsuhashi T, Matsumoto T, Inadama N, Nishikido F, Yoshida E, et al. A sipm-based isotropic-3d pet detector x'tal cube with a three-dimensional array of 1 mm3 crystals. *Phys Med Biol* (2011) 56:6793–807. doi:10.1088/0031-9155/56/21/003

5. Dam HTV, Borghi G, Seifert S, Schaart DR. Sub-200 ps crt in monolithic scintillator pet detectors using digital sipm arrays and maximum likelihood interaction time estimation. *Phys Med Biol* (2013) 58:3243–57. doi:10.1088/0031-9155/58/10/3243

6. Casella C, Heller M, Joram C, Schneider T. A high resolution tof-pet concept with axial geometry and digital sipm readout. *Nucl Instr Methods Phys Res Section A: Acc Spectrometers, Detectors Associated Equipment* (2014) 736:161–8. doi:10.1016/j.nima.2013.10.049

7. Schug D, Lerche C, Weissler B, Gebhardt P, Goldschmidt B, Wehner J, et al. Initial pet performance evaluation of a preclinical insert for pet/mri with digital sipm technology. *Phys Med Biol* (2016) 61:2851–78. doi:10.1088/0031-9155/61/7/2851

8. Lamprou E, Gonzalez-Montoro A, Canizares G, Ilisie V, Sanchez F, Freire M, et al. Tof-pet detectors based on asic technology and analog sipms. In: 2018 IEEE Nuclear Science Symposium and Medical Imaging Conference, NSS/MIC 2018 - Proceedings (2018). p. 1–4. doi:10.1109/NSSMIC.2018.8824517

9. Gundacker S, Turtos RM, Auffray E, Paganoni M, Lecoq P. High-frequency sipm readout advances measured coincidence time resolution limits in tof-pet. *Phys Med Biol* (2019) 64(5):055012. doi:10.1088/1361-6560/aafd52

10. Shimazoe K, Yoshino M, Ohshima Y, Uenomachi M, Oogane K, Orita T, et al. Development of simultaneous pet and compton imaging using gagg-sipm based pixel detectors. *Nucl Instr Methods Phys Res Section A: Acc Spectrometers, Detectors Associated Equipment* (2020) 954:161499. doi:10.1016/j.nima.2018.10.177

11. Lecoq P. Pushing the limits in time-of-flight pet imaging. *IEEE Trans Radiation Plasma Medical Sciences* (2017) 1:473–85. doi:10.1109/trpms.2017.2756674

12. Gundacker S, Auffray E, Jarron P, Meyer T, Lecoq P. On the comparison of analog and digital sipm readout in terms of expected timing performance. *Nucl Instr Methods Phys Res Section A: Acc Spectrometers, Detectors Associated Equipment* (2015) 787:6–11. doi:10.1016/j.nima.2014.10.020

13. Nemallapudi MV, Gundacker S, Lecoq P, Auffray E. Single photon time resolution of state of the art sipms," *Journal Instrumentation* (2016) vol. 11, 10 doi:10.1088/1748-0221/11/10/P10016

14. Gundacker S, Heering A. The silicon photomultiplier: fundamentals and applications of a modern solid-state photon detector. *Phys Med Biol* (2020) 65(17):17TR01. doi:10.1088/1361-6560/ab7b2d

15. Gundacker S, Borghi G, Cherry SR, Gola A, Lee D, Merzi S, et al. On timing-optimized sipms for cherenkov detection to boost low cost time-of-flight pet. *Phys Med Biol* (2023) 68(16):165016. doi:10.1088/1361-6560/ace8ee

16. Anghinolfi F, Jarron P, Martemiyanov A, Usenko E, Wenninger H, Williams M, et al. Nino: an ultra-fast and low-power front-end amplifier/discriminator asic designed for the multigap resistive plate chamber. *Nucl Instr Methods Phys Res Section A: Acc Spectrometers, Detectors Associated Equipment* (2004) 533:183–7. doi:10.1016/j.nima.2004.07.024

17. Nadig V, Gundacker S, Herweg K, Naunheim S, Schug D, Weissler B, et al. Asics in pet: what we have and what we need. *EJNMMI Phys* (2025) 12:16. doi:10.1186/s40658-025-00717-8

18. Francesco AD, Bugalho R, Oliveira L, Pacher L, Rivetti A, Rolo M, et al. Tofpet2: a high-performance asic for time and amplitude measurements of sipm signals in time-of-flight applications. *Journal Instrumentation* (2016) 11(3):C03042. doi:10.1088/1748-0221/11/03/C03042

19. Bugalho R, Francesco AD, Ferramacho L, Leong C, Niknejad T, Oliveira L, et al. Experimental characterization of the tofpet2 asic. *Journal Instrumentation* (2019) 14(3 Mar):P03029. doi:10.1088/1748-0221/14/03/P03029

20. Nadig V, Schug D, Weissler B, Schulz V. Evaluation of the petsys tofpet2 asic in multi-channel coincidence experiments. *EJNMMI Phys* (2021) 8(1):30. doi:10.1186/s40658-021-00370-x

21. Gómez S, Alozy J, Campbell M, Fernandez-Tenllado J, Manera R, Mauricio J, et al. Fastic: a fast integrated circuit for the readout of high performance detectors. *Journal Instrumentation* (2022) 17:C05027. doi:10.1088/1748-0221/17/05/C05027

22. Mariscal-Castilla A, Gómez S, Manera R, Fernández-Tenllado JM, Mauricio J, Kratochwil N, et al. Toward sub-100 ps tof-pet systems employing the fastic asic with analog sipms. *IEEE Trans Radiation Plasma Medical Sciences* (2024) 8(7 Sep):718–33. doi:10.1109/TRPMS.2024.3414578

23. Degenhardt C, Prescher G, Frach T, Thon A, Gruyter Rd, Schmitz A, et al. The digital silicon photomultiplier-a novel sensor for the detection of scintillation light. In: *IEEE nuclear science symposium conference record* (2009). doi:10.1109/NSSMIC.2009.5402190

24. Goldschmidt B, Lerche CW, Solf T, Salomon A, Kiessling F, Schulz V. Towards software-based real-time singles and coincidence processing of digital pet detector raw data. *IEEE Trans Nucl Sci* (2013) 60:1550–9. doi:10.1109/TNS.2013.2252193

25. Gramuglia F, Muntean A, Venialgo E, Lee M-J, Lindner S, Motoyoshi M, et al. Cmos 3d-stacked fsi multi-channel digital sipm for time-of-flight pet applications. In: *2020 IEEE nuclear science symposium and medical imaging conference, NSS/MIC 2020*. Boston, MA: Institute of Electrical and Electronics Engineers Inc. (2020). doi:10.1109/NSS/MIC42677.2020.9507833

26. Pratte JF, Nolet F, Parent S, Vachon F, Roy N, Rossignol T, et al. 3d photon-to-digital converter for radiation instrumentation: motivation and future works. *Sensors* (2021) 21:598–31. doi:10.3390/s21020598

27. Acerbi F, Gundacker S. Understanding and simulating sipms. *Nucl Instr Methods Phys Res Section A: Acc Spectrometers, Detectors Associated Equipment* (2019) 926:16–35. doi:10.1016/j.nima.2018.11.118

28. Lacaita AL, Zappa F, Bigliardi S, Manfredi M. On the bremsstrahlung origin of hot-carrier-induced photons in silicon devices. *Tech Rep* (1993) 40:577–82. doi:10.1109/16.199363

29. Guan Y, Anfimov N, Cao G, Xie Z, Dai Q, Fedoseev D, et al. Study of silicon photomultiplier external cross-talk. *Journal Instrumentation* (2024) 19(6 Jun):P06024. doi:10.1088/1748-0221/19/06/P06024

30. Merzi S, Brunner SE, Gola A, Inglese A, Mazzi A, Paternoster G, et al. Nuv-hd sipms with metal-filled trenches. *Journal Instrumentation* (2023) 18(5):P05040. doi:10.1088/1748-0221/18/05/P05040

31. Lee S, Choong WS, Cates JW. Characterization of external optical crosstalk reduction for sipm-based scintillation detectors with an optical bandpass filter. *Nucl Instr Methods Phys Res Section A: Acc Spectrometers, Detectors Associated Equipment* (2024) 1061(Apr):169101. doi:10.1016/j.nima.2024.169101

32. Kratochwil N, Roncali E, Cates JW, Arino-Estrada G Crosstalk between sipms in dual-ended readout. In: *2024 IEEE nuclear science symposium (NSS), medical imaging conference (MIC) and room temperature semiconductor detector conference (RTSD)* (2024). doi:10.1109/NSS/MIC/RTSD57108.2024.10657276

33. Kratochwil N, Gundacker S, Lecoq P, Auffray E. Pushing cherenkov pet with bgo via coincidence time resolution classification and correction. *Phys Med Biol* (2020) 65(11):115004. doi:10.1088/1361-6560/ab87f9

34. Kratochwil N, Auffray E, Gundacker S. Exploring cherenkov emission of bgo for tof-pet. *IEEE Trans Radiation Plasma Medical Sciences* (2021) 5:619–29. doi:10.1109/TRPMS.2020.3030483

35. Gonzalez-Montoro A, Pourashraf S, Cates JW, Levin CS. Cherenkov radiation-based coincidence time resolution measurements in bgo scintillators. *Front Phys* (2022) 10(Jan). doi:10.3389/fphy.2022.816384

36. Loignon-Houle F, Charlebois SA, Fontaine R, Lecomte R. Monte Carlo simulations of energy, time and spatial evolution of primary electrons generated by 511 kev photons in various scintillators. *Nucl Instr Methods Phys Res Section A: Acc Spectrometers, Detectors Associated Equipment* (2022) 1030:166449–9. doi:10.1016/j.nima.2022.166449

37. Latella R, Gonzalez AJ, Bonifacio DAB, Kovylina M, Griol A, Benlloch JM, et al. Exploiting cherenkov radiation with bgo-based metascintillators. *IEEE Trans Radiation Plasma Medical Sciences* (2023) 7:810–8. doi:10.1109/TRPMS.2023.3310581

38. Herweg K, Nadig V, Bisi S, Bruschini C, Charbon E, Schulz V, et al. Investigating musipms to overcome the limits of bgo in tof-pet. In: *2024 IEEE nuclear science symposium (NSS), medical imaging conference (MIC) and room temperature semiconductor detector conference (RTSD)*. IEEE (2024). p. 1–2. doi:10.1109/NSS/MIC/RTSD57108.2024.10654922

39. Gundacker S, Bruschini C, Gola A, Herweg K, Merzi S, Muntean AA, et al. Digilog: a digital-analog sipm towards 10 ps prompt-photon tagging in tof-pet. In: *2023 IEEE nuclear science symposium, medical imaging conference and international symposium on room-temperature semiconductor detectors (NSS MIC RTSD)*. IEEE (2023). p. 1. doi:10.1109/nssmicrtsd49126.2023.10338522

40. Cates JW, Gundacker S, Auffray E, Lecoq P, Levin CS. Improved single photon time resolution for analog sipms with front end readout that reduces influence of electronic noise. *Phys Med and Biol* (2018) 63(18):185022. doi:10.1088/1361-6560/aadbcd

41. Krake M, Nadig V, Schulz V, Gundacker S. Power-efficient high-frequency readout concepts of sipms for tof-pet and hep. *Nucl Instr Methods Phys Res Section A: Acc Spectrometers, Detectors Associated Equipment* (2022) 1039(Sep):167032. doi:10.1016/j.nima.2022.167032

42. Broadcom. Afbr-s4n22p014m. In: *4 x 4 Nuv-mt silicon photomultiplier array* (2024).

43. Broadcom. Afbr-s4n44p014m nuv-mt single silicon photo multiplier datasheet (2024).

44. Hampel MR, Fuster A, Varela C, Platino M, Almela A, Lucero A, et al. Optical crosstalk in sipms. *Nucl Instr Methods Phys Res Section A: Acc Spectrometers, Detectors Associated Equipment* (2020) 976(Oct):164262. doi:10.1016/j.nima.2020.164262

45. Gola A, Ferri A, Tarolli A, Zorzi N, Piemonte C. Sipm optical crosstalk amplification due to scintillator crystal: effects on timing performance. *Phys Med Biol* (2014) 59:3615–35. doi:10.1088/0031-9155/59/13/3615

46. Kratochwil N, Gundacker S, Auffray E. A roadmap for sole cherenkov radiators with sipms in tof-pet. *Phys Med Biol* (2021) 66(19 Oct):195001. doi:10.1088/1361-6560/ac212a